Atmos. Chem. Phys. Discuss., 14, 27425–27458, 2014
www.atmos-chem-phys-discuss.net/14/27425/2014/
doi:10.5194/acpd-14-27425-2014

Atmospheric Chemistry and Physics Discussions

Parametrization of convective transport in the boundary layer and its impact on the representation of diurnal cycle of wind and dust emissions

F. Hourdin[1], M. Gueye[2], B. Diallo[1], J.-L. Dufresne[1], L. Menut[1], B. Marticoréna[3], G. Siour[3], and F. Guichard[4]

[1]Laboratoire de Météorologie Dynamique, CNRS/IPSL/UMPC, Paris, France
[2]LPAOSF, UCAD, Dakar, Sénégal
[3]LISA, Université Diderot-Paris 7, Créteil, France
[4]CNRM-GAME, CNRS, Toulouse, France

Received: 16 August 2014 – Accepted: 24 September 2014 – Published: 31 October 2014

Correspondence to: F. Hourdin (hourdin@lmd.jussieu.fr)

Published by Copernicus Publications on behalf of the European Geosciences Union.

Abstract

We investigate the impact of the representation of the boundary layer transport in a climate model on the representation of the near surface wind and dust emission, with a focus on the Sahel/Sahara region. We show that the combination of vertical turbulent diffusion with a representation of the thermal cells of the convective boundary layer by a mass flux scheme leads to a more realistic representation of the diurnal cycle of wind in spring, with a maximum near surface wind in the morning. This maximum occurs when the thermal plumes reach the low level jet that forms during the night at a few hundred meters above surface. The horizontal momentum in the jet is transported downward to the surface by compensating subsidences around thermal plumes in typically less than one hour. This leads to a rapid increase of wind speed at surface and therefore of dust emissions owing to the strong non linearity of emission laws. The numerical experiments are performed with a zoomed and nudged configuration of the LMDZ general circulation model, coupled to the emission module of the CHIMERE Chemistry Transport Model, in which winds are relaxed toward that of the ERAI reanalyzes. The new set of parameterizations leads to a strong improvement of the representation of the diurnal cycle of wind when compared to a previous version of LMDZ as well as to the reanalyzes used for nudging themselves. It also reinforces dust emissions in better agreement with observations, but the aerosol optical thickness is still significantly underestimated.

1 Introduction

Desert dust is a secondary but significant contributor to the atmospheric radiative transfer, with regional signature organized around desert area like Sahara, which is estimated to contribute to 25 to 50 % of the global dust emissions (Engelstaedter et al., 2006). This change in radiation may affect the large scale circulation by inducing regional contrasts of several tenth of $W\,m^{-2}$ (Yoshioka et al., 2007; Solmon et al., 2008;

ACPD
14, 27425–27458, 2014

Spyrou et al., 2013), as well as the convective processes in the atmosphere through modulation of the atmospheric static stability. Dust is more and more often taken into account interactively in global climate simulations, such as those coordinated at an international level in the Coupled Model Intercomparison Projects (CMIP, Taylor et al., 2012) that base the anticipation of future climate changes. Dust is a rather simple tracer of atmospheric motions that sediments into the atmosphere more or less rapidly depending on the size of the grains and can be washed out by rainfall. The most uncertain dust-related process is emission which depends non linearly upon the friction velocity U^*. Experiments indicate that dust emissions flux can be considered as a fraction of the "saltation" flux, i. e. the amount of soil material in horizontal movement at the soil surface. The saltation flux can be expressed as a function of a threshold $U^{*\mathrm{Th}}$ and a cubic dependency of the wind friction velocity of the form

$$F_h = \frac{K\rho_a}{g} U^{*3} \left(1 - \frac{U^{*\mathrm{Th}}}{U^*}\right) \left(1 + \frac{U^{*\mathrm{Th}}}{U^*}\right)^2 \quad (1)$$

according to the work of Marticorena and Bergametti (1995b), where K is the eddy diffusivity coefficient and ρ the air density.

The emission thus depends more on the tail of the near surface wind distribution than on the wind mean value. During winter and spring, a large part of dust emissions occurs in the morning (see e.g., Schepanski et al., 2009), which corresponds to a quasi systematic maximum of winds in the observations (Parker et al., 2005; Lothon et al., 2008; Guichard et al., 2009; Schepanski et al., 2009). This maximum is associated with the low level jet which forms at a few hundred meters above the surface, after sunset, consecutively to a collapse of the near boundary layer turbulence (see e.g. Bain et al., 2010; Gounou et al., 2012; Fiedler et al., 2013). After sunrise, a convective boundary layer rapidly develops, which brings momentum from this low level jet down to the surface, and further mixes horizontal momentum on the depth of the convective boundary layer, typically 2 to 6 km thick over Sahara and Sahel (see e.g. Cuesta et al., 2009). Todd et al. (2008) report problems in the representation of the diurnal cycle of

ACPD
14, 27425–27458, 2014

near surface wind in a series of simulations with regional models over the Bodélé region during the Bodex 2005 experiment. They also conclude that the problem comes more from missing physics in the model than from the grid resolution. This diurnal cycle is neither well captured in the ERA-Interim reanalyzes (Fiedler et al., 2013) nor in other state-of-the-art reanalyzes datasets as recently shown by Largeron et al. (2014). Fiedler et al. (2013) report typical underestimation of 24–50 % for the jet maximum velocity in the Bodele region. Todd et al. (2008) and Knippertz and Todd (2012) underline the importance of a good representation of the boundary layer transport, contrast between nocturnal turbulence in a stable atmosphere and convective transport during the day being a key for the representation of this nocturnal jet and its impact on surface wind.

Various approaches have been proposed in the past decades to represent boundary layer convection. Deardorff (1970) first noticed that parameterizations of boundary layer turbulence that are based on eddy- or K-diffusion fail to represent the basics of boundary layer convection, which essentially transports heat upward from the surface, i. e. upward the gradient of potential temperature since the atmosphere is generally neutral or even somewhat stable above the first few hundred meters which corresponds to the (unstable) surface layer. The counter-gradient term he proposed to reconcile the diffusive formulations with convection conditions was later on given a more explicit formulation based on the non local aspect of convective transport by Troen and Mahrt (1986) and by Holtslag and Boville (1993). Stull (1984) underlined the importance of non local aspects and proposed the "transilience matrices" framework. Chatfield and Brost (1987) first proposed to combine a diffusive approach with a "mass flux" scheme dedicated to the representation of the boundary layer convection. In this approach, the convection is represented by splitting the atmospheric column in two compartments, one associated with the concentrated buoyant updrafts (or thermal plumes) that raise from the surface and the other one to compensating subsidence around those plumes. This approach was developed independently by two teams and since adopted in several groups (Hourdin et al., 2002; Soares et al., 2004; Siebesma et al., 2007; Pergaud

ACPD
14, 27425–27458, 2014

et al., 2009; Angevine et al., 2010; Neggers et al., 2009; Neggers, 2009; Hourdin et al., 2013b). It has been shown in particular to open the way to quite accurate representation of cumulus clouds that form at the top of convective thermal plumes (Rio and Hourdin, 2008; Jam et al., 2013). The first application of these ideas to the simulation of the dry convective boundary layer (Hourdin et al., 2002) demonstrated the capability of the so-called "thermal plume model" to correctly represent the up-gradient transport of heat in a slightly stable convective mixed layer. This approach was shown to capture well also the contrast between the very thin nocturnal boundary layer, in which the turbulent diffusion alone is at work, and daily conditions in which the role of turbulent diffusion is confined to the surface layer while the mass flux accounts for most part of the turbulent transport in the mixed layer. This thermal plume model was developed for the LMDZ atmospheric general circulation model, in which it was activated in particular to perform a sub-set of climate simulations for the last CMIP5 exercise (Hourdin et al., 2013b).

The present study aims at exploring the impact of those new parameterizations on the representation of dust emission and transport, and anticipate future versions of the climate simulations with interactive aerosols. For this, the emission module from the Chemistry Transport Model CHIMERE (Menut et al., 2013) was coupled to the climate model. We show here how the activation of the thermal plume model leads to a better representation of the diurnal cycle of near surface winds – even better than in current meteorological reanalyzes – and how this better representation reinforces surface emissions drastically. We focus here on emissions during the dry season while a companion paper will be devoted to the representation of dust emission by gusts associated with convection generated cold pools, for which a specific parametrization has been introduced also in LMDZ (Grandpeix and Lafore, 2010; Rio et al., 2009).

In Sect. 2, we present the model setup. We then illustrate the impact of the parameterization of the boundary layer on the near surface wind distribution and dust emission using online dust simulations with two versions of the LMDZ physical package (Sect. 3) and compare the results with site observations (Sect. 4), before analyzing in more de-

ACPD
14, 27425–27458, 2014

tail the representation of the mean diurnal cycle of near surface wind over the Sahel when the thermal plume model is activated (Sect. 5) and drawing some conclusions.

2 Model description and simulation setup

2.1 LMDZ5 and IPSL-CM5

The LMDZ dynamical core is based on a mixed finite difference/finite volume discretization of the primitive equations of meteorology and conservation equations for trace species. It is coupled to a set of physical parameterizations. Two versions of the model, LMDZ5A and LMDZ5B, are considered here that differ by the activation of a different set of parameterizations for turbulence, convection and clouds. In the "Standard Physics" package SP used in version LMDZ5A (Hourdin et al., 2013a), boundary layer turbulence is parameterized as a diffusion with an eddy diffusivity that depends on the local Richardson number. A counter-gradient term on potential temperature (Deardorff, 1972) as well as a dry convective adjustment are added to handle dry convection cases which often prevail in the boundary layer. In the "New Physics" package NP of version LMDZ5B (Hourdin et al., 2013b), the vertical transport in the boundary layer relies on the combination of a classical parameterization of turbulent diffusion with the thermal plume model introduced above (Hourdin et al., 2002; Rio and Hourdin, 2008). The SP and NP versions also differ by the representation of deep convection closure and triggering. However, we will concentrate the present study on the dry season over West Africa when deep convection does not activate. The two versions correspond to the IPSL-CM5A and -CM5B versions of the IPSL coupled model used for CMIP5 (Dufresne et al., 2013).

2.2 The "thermal plume model"

In the NP version, eddy diffusivity K_z is computed based on a prognostic equation for the turbulent kinetic energy that follows Yamada (1983). It is mainly active in practice in

ACPD
14, 27425–27458, 2014

the surface boundary layer, typically in the first few hundred meters above surface. It is combined with a mass flux scheme that represents an ensemble of coherent ascending thermal plumes as a mean plume. A model column is separated in two parts: the thermal plume and its environment. The vertical mass flux in the plume $f_{th} = \rho \alpha_{th} w_{th}$ – where ρ is the air density, w_{th} the vertical velocity in the plume and α_{th} its fractional coverage – varies vertically as a function of lateral entrainment e_{th} (from environment to the plume) and detrainment d_{th} (from the plume to the environment). For a scalar quantity q (total water, potential temperatures, chemical species, aerosols), the vertical transport by the thermal plume reads

$$\frac{\partial f_{th} q_{th}}{\partial z} = e_{th} q - d_{th} q_{th} \tag{2}$$

q_{th} being the concentration of q inside the plume. Note that this formulation assumes stationarity of the plume properties when compared to the time scale of the change in large scale model variables, a classical approximation in parameterizations of convective motions. Here air is assumed to enter the plume with the concentration of the large scale, which is equivalent to neglect the plume fraction α_{th} in this part of the computation. The particular case of $q \equiv q_{th} \equiv 1$ gives the continuity equation that relates e_{th}, d_{th} and f_{th}. The vertical velocity w_{th} in the plume is driven by the plume buoyancy $g(\theta_{th} - \theta)/\theta$. The computation of w_{th}, α_{th}, e_{th} and d_{th} is a critical part of the code. We use here the version of the scheme described by Rio et al. (2010) and used in LMDZ5B (Hourdin et al., 2013b).

Finally, for both the SP and NP versions, the time evolution of q reads

$$\frac{\partial q}{\partial t} = -\frac{\partial \overline{\rho w' q'}}{\partial z} \tag{3}$$

with

$$\overline{\rho w' q'} = f_{th}(q - q_{th}) - \rho K_z \left(\frac{\partial q}{\partial z} - \Gamma \right) \tag{4}$$

ACPD
14, 27425–27458, 2014

In the SP version, $f_{th} \equiv 0$, the computation of K_z is based on an equilibrium TKE equation which leads to a Richardson dependent formulation, while the counter-gradient Γ is introduced for transport of potential temperature. In the NP version, $\Gamma \equiv 0$, K_z is computed from a TKE prognostic equation and f_{th} accounts for the thermal plumes.

Note that the same equation is applied for the time evolution of the horizontal component of the specific momentum u and v, but with an optional additional term in the plume equation, that accounts for the exchange of momentum by pressure torque following Hourdin et al. (2002). This optional term has a very minor impact on the results and is not activated in the present simulations for the sake of simplicity.

2.3 The CHIMERE dust emission module

Mineral dust injection in the atmosphere is computed using CHIMERE emission modules (Menut et al., 2013). The configuration is the one used in Menut et al. (2009) for the AMMA experiment. Dust emissions depend on the soil and surface properties and on the near-surface meteorology with the friction velocity. Soil and surface properties are issued from a $1^\circ \times 1^\circ$ database that covers North Africa including Sahara and Sahel available at http://www.lisa.u-pec.fr/mod/data/index.php. The saltation flux is estimated following the Marticorena and Bergametti (1995a) scheme (see also Marticorena et al., 1997; Callot et al., 2000) and the sandblasting with the Alfaro and Gomes (2001) scheme, optimized following Menut et al. (2005). The threshold for the friction velocity is estimated using the Shao and Lu (2000) scheme and to account for sub-grid scale variability of the mean wind speed, a Weibull distribution is used (Cakmur et al., 2004).

Coupling of LMDZ with the CHIMERE emission module follows the way CHIMERE is currently forced by regional climate models: an effective wind U_{eff} is used instead of the large scale wind interpolated at the 10 m height, U_{10m}. Folowing Beljaars and Viterbo (1994), this effective wind is computed by adding a convective vertical velocity W^*, $U_{eff}^2 = U_{10m}^2 + 1.2W^{*2}$ that aims at accounting for the wind gustiness in a statistically unstable atmosphere. Both U_{10m} and W^* are computed by LMDZ. For the SP

ACPD
14, 27425–27458, 2014

version, W^* is estimated directly from the sensible heat flux $\overline{w'\theta'}_0$ at the surface as $W^* = \left(gh\overline{w'\theta'}_0/\theta\right)^{1/3}$ where h is the boundary layer depth, g the gravity and θ the potential temperature in the first model layer. For the NP version, we use either the same computation of W^* or directly the thermal plume velocity w_{th}, both computation giving very similar results. The second option is retained for the simulations shown here. In addition, a Weibull parameterization is used to account for the effect of spatial inhomogeneities of wind speed within a grid mesh.

The diameter of emitted dust particles ranges typically from a few nanometers to micrometers. In order to accurately describe this size distribution both in number of particles and in mass, it is common to describe the large range of aerosols sizes using bins and with a distribution following a logarithmic increase (Seinfeld and Pandis, 1998). In the model, the aerosol distribution is represented by a mean mass median diameter, D_p, for each bin. For specific studies on emissions and transport of mineral dust, it has been shown that 12 bins corresponds to a good compromise between accuracy and computational cost for long-range transport model simulations (Forêt et al., 2006; Menut et al., 2007). Settling of dust particles and dry deposition are computed as in CHIMERE. Scavenging is also activated in the model but it is not involved in the results presented here, before the monsoon onset.

2.4 Model configuration and simulations

In order to assess the representation of emission and turbulent processes, the model is run with its zooming capability in a nudged mode. The use of the zoomed/nudged version for model evaluation was described in details by Coindreau et al. (2007).

The zoom consists in a refinement of the longitude and latitude discretization. Here, the zoom covers West Africa and the tropical Atlantic ocean. In order to limit interpolation issues for soil properties, the zoom was chosen so as to get a quasi uniform $1^\circ \times 1^\circ$ resolution over a (70° W–30° E; 10° S–40° N) longitude-latitude box, close to the CHIMERE data set resolution. Nevertheless, the points of the LMDZ grid do not exactly

ACPD
14, 27425–27458, 2014

match those of the CHIMERE dust model. First tests have shown that a linear interpolation considerably degrades the results. A nearest neighbor method was retained instead that provides much better results.

The LMDZ model is most commonly used in climate mode: integrated from an initial state just imposing some boundary conditions such as insolation, sea surface temperature (in stand-alone atmospheric configurations), composition of dry air, etc. For validation of subcomponents of the model as is the case here, it can be desirable to force the model to follow the observed synoptic meteorological situation, by nudging (relaxing) the model meteorology toward observations. That way, errors coming from the deficiencies of the subcomponent can be distinguished from those that arise from the erroneous representation of the atmospheric circulation in the model. This also allows a direct day-by-day comparison with observations as illustrated by Coindreau et al. (2007). In practice here, winds are relaxed toward ERA-Interim re-analyzes of the European Centre for Medium-Range Weather Forecasts (ECMWF), by adding a non-physical relaxation term to the model equations:

$$\frac{\partial X}{\partial t} = F(X) + \frac{X^{\mathrm{a}} - X}{\tau} \tag{5}$$

where X stands for u and v wind components, X^{a} their values in the reanalyzes, F is the operator describing the dynamical and physical processes that determine the evolution of X, and τ is the time constant.

Before applying relaxation, ERAI data are interpolated on the horizontal stretched-grid of the LMDZ model as well as on the hybrid σ-p vertical coordinates. At each model time step also, the ERAI data are interpolated linearly in time between two consecutive states, evalable each 6 h in the dataset used here. Different time constants can be used inside and outside the zoomed region (with a smooth transition between the inner and outer region that follows the grid cell size). Here, the constant outside the zoom is 3 h. Inside the zoom tests were made with values ranging from 1 to 120 h. The longer the time constant the weakest the constraint by the analyzed wind fields. We

ACPD
14, 27425–27458, 2014

focus here on simulations with τ = 3 h, named SP3 and NP3 depending on the physical package used, as well as on a sensitivity test NP48 ran with the NP version and τ = 48 h. The initial state of the simulations is taken from a multi-annual spin-up simulation with interactif dust that corresponds to 1 December 2005.

3 Dependency of dust lifting to the representation of wind

We first present in Fig. 1 the average emission (colored shading) for March 2006 obtained in the SP3 (top) and NP3 (bottom) simulations. The zoomed grid is apparent on the right hand side of the lower panel from the distortion of the color rectangles, each corresponding to a grid cell. The contours corresponds to the Aerosol Optical Thickness at 550 nm (noted AOT afterward in the paper). The NP3 and SP3 emissions are essentially located in the same areas, but they are much stronger for the NP version. The total Saharan emission for March 2006 is of 18 Mt for the SP and 75 Mt for the NP version. The latter value is already in the lower range of current estimates of the climatolgical total dust emission by North Africa for March (see e.g. Figure 6 of Laurent et al., 2008). As a consequence of the stronger emissions, the AOTs are also by a factor about 4 larger for the NP than for the SP version. Note that even the NP3 simulation underestimates the actual AOT as illustrated later on.

In order to interpret at process level the origin of the difference in emission between the two simulations, we show in Fig. 2 a scatter plot of the emission and wind intensity for a grid cell in the main emission area in Mauritania (location (7.5° W, 18.5° N) shown in red in Fig. 1). The left panel of the figure corresponds to instantaneous values sampled hourly during the month. The cubic relationship used for emission computation is directly visible on this graph, and the same relationship is clearly exhibited for both simulations but the wind distributions markedly differ. Indeed, the maximum speeds explored by the SP version never exceed 10 m s^{-1} while the wind distribution for the NP version explores much larger values.

ACPD
14, 27425–27458, 2014

At the opposite, when the emissions are related to the daily-mean wind speed (right panel of Fig. 2) it appears that the wind explored are on average weaker in the NP than in the SP version. However, even for rather moderate values of the wind of 4 to 6 m s^{-1}, the NP version exhibits significant emissions while the SP does not. It is thus the sub-diurnal distribution of the wind which explains the difference between the emissions of the two versions.

This is confirmed when focusing on time series of emissions and wind speed at the same grid point for 2 to 13 March (Fig. 3), a period which includes the strongest observed dust event of that particular month (Slingo et al., 2006). Thanks to nudging, both simulations follow a similar evolution of the wind at daily scale with a maximum between 6 and 8 March which correspond to this dust event. However, the NP3 simulation shows a marked peak each morning while the SP3 simulation does not. Because of the strong non linearity of the emission process, this morning peak reinforces emissions during the major dust event and also often produces emissions in the morning when the SP3 simulations does not predict any.

4 Comparison with site observations

For evaluation of the representation of the above mentioned processes, we compare the model results with observations recorded at surface stations installed in the framework of the AMMA project (Redelsperger et al., 2006). A set of three stations dedicated to the monitoring of mineral dust were deployed in 2006 along a "Sahelian Dust Transect" (Marticorena et al., 2010). The stations are aligned between 13 and 15° N along the main pathway of the Saharan and Sahelian dust toward the Atlantic Ocean, namely Banizoumbou (Niger, 13.54° N, 2.66° E), Cinzana (Mali, 13.28° N, 5.93° W) and M'Bour (Senegal, 14.39° N, 16.96° W). The locations of the three stations are displayed in Fig. 1 as black rectangles. In addition to the local meteorology (wind speed and direction, air temperature, relative humidity), the atmospheric concentration of Particulate Matter smaller than 10 µm (PM_{10} concentration) is continuously monitored with a 5 min

ACPD
14, 27425–27458, 2014

time step. The AOT is measured by a sunphotometer from the AERONET/PHOTONS network.

Although the stations are not located in the emission area discussed above, model results show very similar diurnal variations of wind at these sites. We here consider the full 2005–2006 winter, from December to March. The comparison is done for the three simulations: SP3, NP3 and NP48. We show in the top panels of Fig. 4, for Cinzana and Banizoumbou, the evolution of the daily averaged wind. There is a reasonable agreement between models and observations as for the order of magnitude of this mean wind. All the simulations tend however to slightly overestimate the wind at Cinzana and underestimate it at Banizoumbou. Differences between the three simulations are generally small, with a tendency of SP3 to simulate slightly stronger winds, especially at Cinzana, similarly to what was seen in the right panel of Fig. 2. The day-to-day variations of the wind closely follow observations, which illustrates that relevant information at synoptic scales present in ERAI reanalyzis are passed to the numerical experiments through the nudging procedure.

The fact that the NP48 simulation does not depart that much from NP3 suggests that nudging with a 48 h time constant is in fact strong enough to constrain the model day-to-day variations.

The middle panels in the same figure show the maximum value for each day. Consistently with Fig. 3, the NP version of the model produces much larger maximum winds than the SP version. Those winds are in fact larger than observations at Cinzana (where the SP3 version is closer to observations) and close to observations at Banizoumbou. However, when considering the ratio of the maximum to mean winds, it is for both stations the NP versions that give the best results. It is consistent with an idea that this relative variation of wind within a day is more controlled by physical processes and less subject to large scale biases (whatever they are) than the absolute mean value and mean field.

As for dust evaluation, we first show in Fig. 5 the comparison of the observed and modeled PM_{10} surface concentration and AOT at 550 nm (computed following Moulin

ACPD
14, 27425–27458, 2014

et al., 2001) at M'Bour, close to Dakar/Senegal. This station is considered at first because it is downstream of the dust emissions discussed in the previous section. The synoptic behavior is captured reasonably well by the model, and in particular the occurrence of the main dust event of the winter in early March. This once again reflects that some information on the actual circulation is transmitted to the simulation thanks to nudging by reanalyzes. The concentrations and emissions are however typically underestimated by a factor of 2 in the NP simulations, the SP version being even farther from observations. Note that there is also a significant and systematic increase of dust when weakening the nudging, going from $\tau = 3$ h to 48 h.

A more systematic and synthetic comparison is shown in Fig. 6 for the three stations in form of a scatter-plot of observed vs. simulated AOT. The underestimation of AOTs is clearly present at the three stations, and it is even somewhat worse at Cinzana and Banizoumbou. The behavior is however similar in terms of comparison of the three simulations: AOTs are always larger for the NP than for the SP physics, and increase when weakening the nudging (from NP3 to NP48). Note that the improvement is significant both for the weak (associated with small lifting events) and strong concentrations. The fact that the improvement is slightly smaller for large values is consistent with the larger role played by large scale dynamics for those events. But even then, the representation of the diurnal cycle of winds plays a significant role.

Several factors can explain the overall underestimations of AOTs and concentrations but this discussion is out of the scope of the present paper and will deserve further investigations.

5 Mean diurnal cycle of boundary layer wind

We finally analyze the representation of the diurnal cycle of wind. We show in Fig. 7 the mean diurnal cycle of the near surface wind at Cinzana and Banizoumbou for the full winter period (December 2005 to March 2006). Note that this diurnal cycle is very similar whatever the period selected within the winter season and whatever the year

ACPD
14, 27425–27458, 2014

considered.[1] This diurnal cycle is better represented in the NP than in the SP version, and also better represented than in the reanalyzes used for nudging. The rather poor representation of the diurnal cycle of wind in ERAI as well as in other reanalyzes datasets was recently pointed out by Largeron et al. (2014).

The tendency of the NP simulations to over-predict winds at Cizana and under-predict them at Banizoumbou, already visible in Fig. 4, may have several explanations: effect of local subgrid-sale topography, bad prediction of the local drag which is taken directly from the climate model boundary conditions and not from the more accurate database used to compute emissions, bias in the reanalyzes winds used for nudging... More surprising is the fact that ERA reanalyzes almost systematically over-estimate wind speed, which may have practical implication for dust transport computations. In particular, tuning of emission algorithms with overestimated winds from reanalyzes may lead to artificially underestimate the emissions when better winds are given to the emission module, as is the case here.

The differences seen in Fig. 7 for the 10 m wind diurnal cycle between simulations and reanalyzes reflects strong differences in the vertical too. We show in Fig. 8 the vertical profiles at 6 a.m. (left) and noon (right) for Banizoumbou.[2] At the end of the night, the jet is much stronger in the NP version than in the reanalyzes, as well as its decoupling from the surface. Note that a similar underestimation of the ERAI low level jet intensity is shown in Fig. 4 of Fiedler et al. (2013), when compared to observations in the Bodele region. At the opposite, the wind is much better mixed within the boundary layer at noon in the NP simulations while the reanalyzes keep the signature of the low level jet. Note the similarity of the SP version with the reanalysis, which may be related to the fact that both the SP version of LMDZ and the ECMWF model used to produce

[1] The diurnal cycle at M'bour (not shown) displays a similar cycle with maximum in the morning, but not as marked, probably because the land–sea contrasts maintain a significant amount of wind even during the night.

[2] The profiles are very similar for Cinzana and not that different for M'Bour (not shown).

ACPD
14, 27425–27458, 2014

the reanalysis, base there boundary layer computation on eddy diffusion approaches, without accounting for the non local transport by thermal plumes.

The vertical mixing of horizontal momentum by thermal cells is key for the representation of the nocturnal jet and near surface wind in the NP simulation. We present in the upper panel of Fig. 9 for four consecutive days, the vertical profile of the module $\|V\| = \sqrt{u^2 + v^2}$ of the horizontal wind in black contours, together with the tendency of this module due to the thermal plume model (color shadings)

$$\frac{\partial \|V\|}{\partial t}_{|\mathrm{th}} = \frac{1}{\|V\|}\left(u\frac{\partial u}{\partial t}_{|\mathrm{th}} + v\frac{\partial v}{\partial t}_{|\mathrm{th}}\right) \quad (6)$$

The top of the turbulent boundary layer is also identified on the graphs as a red curve. Following a classical approach (see e.g. Hourdin et al., 2002), the curve corresponds to $Ri_b = 0.25$, where

$$Ri_b = \frac{gz}{\theta}\frac{\theta - \theta_s}{\|V\|^2} \quad (7)$$

is a so-called bulk Richardson number (similar to a gradient Richardson number but computed non locally by replacing gradient terms by finite differences between altitude z with a potential temperature θ and surface with a temperature θ_s, where the wind is assumed to vanish). During the day, the momentum is well mixed within the full convective boundary layer which grows as high as 5 km, with vertical winds in the thermal plumes of the order of $2\,\mathrm{m\,s^{-1}}$. The collapse of the boundary layer at sunset is very rapid. There is essentially no turbulence left after 18:00. The wind, decoupled from the surface, then starts to accelerate, driven by the unbalance between the Coriolis force and horizontal pressure gradient (which evolves itself in response to the diurnal cycle of the thermal forcing of the monsoon flow, Parker et al., 2005). The jet maximum intensity varies from about 8 to $25\,\mathrm{m\,s^{-1}}$ and the height of the jet core from 200 to 500 m depending on the night considered. The strong wind shear created at the surface

ACPD
14, 27425–27458, 2014

gradually produces turbulence in the surface layer, but it is only at sunrise that the boundary layer rapidly develops. The thermal convection starts at 08:30 LT and reaches 1 km before 10:00 LT. Because the shear in momentum is very strong at the beginning, the impact of vertical transport by the thermal plume model is also very large. The wind speed at surface can increase by up to 25 m s^{-1} in only one hour in the first model layer (middle panel). The peak is very short in time (less than one hour). With a typical updraft velocity $w_{th} \simeq 1$ m s^{-1} at the height of the nocturnal jet and an horizontal fraction of the surface covered by thermal plumes α_{th} of typically 0.1 to 0.2, the compensating subsidence (10–20 cm s^{-1} typically) needs less than one hour to bring the air from the jet core (200–500 m) down to the surface.

It is this peak of downward transport from the nocturnal jet which explains the morning peak in near surface wind. The mixing also rapidly reduces the jet intensity. The thermals still accelerates the surface layer as long as the boundary deepens in the morning. The near surface wind slowly decreases afterward, until late afternoon. As shown by the green curve in the second panel of Fig. 9, this decrease is the consequence of turbulent exchange with the surface. The acceleration by thermals is then smaller because of the reduced vertical gradients in the mixed layer.

6 Conclusions

This study focuses on the impact of the representation of boundary layer processes on near surface wind and on dust emissions. Significant conclusions may be drawn that do not depend on the particular model used for representation of dust (as soon as it accounts for the strong non linearity of emission to near surface wind).

1. This study underlines the importance of a correct representation of the vertical transport of horizontal momentum by boundary layer processes for a good representation of the diurnal cycle of wind at the surface.

ACPD
14, 27425–27458, 2014

2. It clearly attributes the observed morning peak of near surface wind to the downward transport of momentum by the compensating subsidence of thermal plumes, at there first stage, when they reach the height of the low-level jet which develops during the night at a few hundred meters above the surface, when the wind is decoupled from the surface.

3. This study advocates for the representation of vertical boundary layer transport through the combination of eddy diffusion and mass flux representation of the coherent structures of the convective boundary layer, an approach first proposed by Chatfield and Brost (1987). It confirms in particular the ability of the the so-called thermal plume model to represent in a physical way the vertical transport of momentum, as already illustrated in Fig. 2 of Hourdin et al. (2002), based on comparison of single-column computations with Large Eddy Simulations results issued from an inter-comparison study coordinated by Ayotte et al. (1996).

4. The diurnal cycle of the near surface wind is well captured in the NP version of the LMDZ model that includes these thermal plume processes, and much better represented than in the reanalyzes used for nudging. This conclusion goes beyond this particular model since many chemistry transport models rely on reanalyzes for the computation of near surface wind.

5. An important practical consequence of this point is that it could be better to use much larger time constants for nudging than what was currently believed. The rationale for using time constants of a few hours was to let the rapid processes represented in turbulent parameterizations to express themselves, without departing from the observed synoptic situation. The problem is that the time constants which prevail for the creation and control of the nocturnal jet are typically those of the diurnal cycle itself. So constants larger than one day should be used for this particular problem. It seems that with time constants as large as 48 h the synoptic situation is still rather well constraint, which probably points to a reasonable be-

ACPD
14, 27425–27458, 2014

havior of the physics of the LMDZ model which does not tend to depart too fast from the observed situation.

Despite a reasonable representation of the near surface winds (at least at the stations available, which unfortunately are not in the main emission zones), the model seriously underestimates the observed dust loading of the atmosphere, typically by a factor of 2 for the NP48 simulation that shows the strongest emissions. Such discrepancies are however not that exceptional for simulations of African desert dust (e.g., Todd et al., 2008).

The discussion was focused here on year 2006 but the comparison was extended on the following years (for which the same observation are available) leading to very similar results. Note that the model already includes a Weibull parameterization to account for the effect of spatial inhomogeneities of wind speed within a grid mesh. Of course many points could be investigated to try to understand the origin of this underestimation. Whatever those points, it does not alter the main result of the paper which is that an accurate representation of the diurnal evolution of the boundary layer and transport of momentum by boundary layer convective cells must be taken into account for a good representation of winds, and that such a good representation is accessible now to the modeling community.

Acknowledgements. We thank Bernadette Chatenet, the technical PI of the Sahelian stations from 2006 to 2012, Jean-Louis Rajot, the scientific co-PI and the African technicians who manage the stations: M. Coulibaly and I. Koné from the Institut d'Economie Rurale in Cinzana, Mali and A. Maman and A. Zakou from the Institut de Recherche pour le Développement, Niamey, Niger.

References

Alfaro, S. C. and Gomes, L.: Modeling mineral aerosol production by wind erosion: emission intensities and aerosol size distribution in source areas, J. Geophys. Res., 106, 18075–18084, 2001. 27432

ACPD
14, 27425–27458, 2014

Angevine, W. M., Jiang, H., and Mauritsen, T.: Performance of an eddy diffusivity-mass flux scheme for shallow cumulus boundary layers, Mon. Weather Rev., 138, 2895–2912, 2010. 27429

Ayotte, K. W., Sullivan, P. P., Andrén, A., Doney, S. C., Holtslag, A. A., Large, W. G., McWilliams, J. C., Moeng, C.-N., Otte, M. J., Tribbia, J. J., and Wyngaard, J. C.: An evaluation of neutral and convective planetary boundary-layer parameterizations relative to large eddy simulations, Bound.-Lay. Meteorol., 79, 131–175, 1996. 27442

Bain, C. L., Parker, D. J., Taylor, C. M., Kergoat, L., and Guichard, F.: Observations of the Nocturnal Boundary Layer Associated with the West African Monsoon, Mon. Weather Rev., 138, 3142–3156, doi:10.1175/2010MWR3287.1, 2010. 27427

Beljaars, A. C. M. and Viterbo, P.: The sensitivity of winter evaporation to the formulation of aerodynamic resistance in the ECMWF model, Bound.-Lay. Meteorol., 71, 135–149, doi:10.1007/BF00709223, 1994. 27432

Cakmur, R. V., Miller, R. L., and Torres, O.: Incorporating the effect of small-scale circulations upon dust emission in an atmospheric general circulation model, J. Geophys. Res., 109, D07201, doi:10.1029/2003JD004067, 2004. 27432

Callot, Y., Marticorena, B., and Bergametti, G.: Geomorphologic approach for modelling the surface features of arid environments in a model of dust emissions: application to the Sahara desert, Geodin. Acta., 13, 245–270, doi:10.1016/S0985-3111(00)01044-5, 2000. 27432

Chatfield, R. B. and Brost, R. A.: A two-stream model of the vertical transport of trace species in the convective boundary layer, J. Geophys. Res., 92, 13263–13276, 1987. 27428, 27442

Coindreau, O., Hourdin, F., Haeffelin, M., Mathieu, A., and Rio, C.: A global climate model with strechable grid and nudging: a tool for assesment of physical parametrizations, Mon. Weather Rev., 135, 1474–1489, 2007. 27433, 27434

Cuesta, J., Marsham, J. H., Parker, D. J., and Flamant, C.: Dynamical mechanisms controlling the vertical redistribution of dust and the thermodynamic structure of the West Saharan atmospheric boundary layer during summer, Atmos. Sci. Lett., 10, 34–42, doi:10.1002/asl.207, 2009. 27427

Deardorff, J. W.: Preliminary results from numerical integrations of the unstable planetary boundary layer, J. Atmos. Sci., 27, 1209–1211, 1970. 27428

Deardorff, J. W.: Theoretical expression for the countergradient vertical heat flux, J. Geophys. Res., 77, 5900–5904, 1972. 27430

ACPD
14, 27425–27458, 2014

Dufresne, J.-L., Foujols, M.-A., Denvil, S., Caubel, A., Marti, O., Aumont, O., Balkanski, Y., Bekki, S., Bellenger, H., Benshila, R., Bony, S., Bopp, L., Braconnot, P., Brockmann, P., Cadule, P., Cheruy, F., Codron, F., Cozic, A., Cugnet, D., de Noblet, N., Duvel, J.-P., Ethé, C., Fairhead, L., Fichefet, T., Flavoni, S., Friedlingstein, P., Grandpeix, J.-Y., Guez, L., Guilyardi, E., Hauglustaine, D., Hourdin, F., Idelkadi, A., Ghattas, J., Joussaume, S., Kageyama, M., Krinner, G., Labetoulle, S., Lahellec, A., Lefebvre, M.-P., Lefevre, F., Levy, C., Li, Z. X., Lloyd, J., Lott, F., Madec, G., Mancip, M., Marchand, M., Masson, S., Meurdesoif, Y., Mignot, J., Musat, I., Parouty, S., Polcher, J., Rio, C., Schulz, M., Swingedouw, D., Szopa, S., Talandier, C., Terray, P., Viovy, N., and Vuichard, N.: Climate change projections using the IPSL-CM5 Earth System Model: from CMIP3 to CMIP5, Clim. Dynam., 40, 2123–2165, doi:10.1007/s00382-012-1636-1, 2013. 27430

Engelstaedter, S., Tegen, I., and Washington, R.: North African dust emissions and transport, Earth-Sci. Rev., 79, 73–100, doi:10.1016/j.earscirev.2006.06.004, 2006. 27426

Fiedler, S., Schepanski, K., Heinold, B., Knippertz, P., and Tegen, I.: Climatology of nocturnal low-level jets over North Africa and implications for modeling mineral dust emission, J. Geophys. Res., 118, 6100–6121, doi:10.1002/jgrd.50394, 2013. 27427, 27428, 27439

Forêt, G., Bergametti, G., Dulac, F., and Menut, L.: An optimized particle size bin scheme for modeling mineral dust aerosol, J. Geophys. Res., 111, D17310, doi:10.1029/2005JD006797, 2006. 27433

Gounou, A., Guichard, F., and Couvreux, F.: Observations of diurnal cycles over a West African meridional transect: pre-monsoon and full-monsoon seasons, Bound.-Lay. Meteorol., 144, 329–357, doi:10.1007/s10546-012-9723-8, 2012. 27427

Grandpeix, J. and Lafore, J.: A density current parameterization coupled with Emanuel's convection scheme, Part I: The models, J. Atmos. Sci., 67, 881–897, doi:10.1175/2009JAS3044.1, 2010. 27429

Guichard, F., Kergoat, L., Mougin, E., Timouk, F., Baup, F., Hiernaux, P., and Lavenu, F.: Surface thermodynamics and radiative budget in the Sahelian Gourma: Seasonal and diurnal cycles, J. Hydrol., 375, 161–177, doi:10.1016/j.jhydrol.2008.09.007, 2009. 27427

Holtslag, A. A. M. and Boville, B. A.: Local versus non-local boundary-layer diffusion in a global climate model, J. Climate, 6, 1825–1842, 1993. 27428

Hourdin, F., Couvreux, F., and Menut, L.: Parameterisation of the dry convective boundary layer based on a mass flux representation of thermals, J. Atmos. Sci., 59, 1105–1123, 2002. 27428, 27429, 27430, 27432, 27440, 27442

ACPD
14, 27425–27458, 2014

Hourdin, F., Foujols, M.-A., Codron, F., Guemas, V., Dufresne, J.-L., Bony, S., Denvil, S., Guez, L., Lott, F., Ghattas, J., Braconnot, P., Marti, O., Meurdesoif, Y., and Bopp, L.: Impact of the LMDZ atmospheric grid configuration on the climate and sensitivity of the IPSL-CM5A coupled model, Clim. Dyn., 40, 2167–2192, doi:10.1007/s00382-012-1411-3, 2013a. 27430

Hourdin, F., Grandpeix, J.-Y., Rio, C., Bony, S., Jam, A., Cheruy, F., Rochetin, N., Fairhead, L., Idelkadi, A., Musat, I., Dufresne, J.-L., Lahellec, A., Lefebvre, M.-P., and Roehrig, R.: LMDZ5B: the atmospheric component of the IPSL climate model with revisited parameterizations for clouds and convection, Clim. Dyn., 40, 2193–2222, doi:10.1007/s00382-012-1343-y, 2013b. 27429, 27430, 27431

Jam, A., Hourdin, F., Rio, C., and Couvreux, F.: Resolved versus parametrized boundary-layer plumes, Part III: Derivation of a statistical scheme for cumulus clouds, Bound.-Lay. Meteorol., 147, 421–441, doi:10.1007/s10546-012-9789-3, 2013. 27429

Knippertz, P. and Todd, M. C.: Mineral dust aerosols over the Sahara: meteorological controls on emission and transport and implications for modeling, Rev. Geophys., 50, RG1007, doi:10.1029/2011RG000362, 2012. 27428

Laurent, B., Marticorena, B., Bergametti, G., LéOn, J. F., and Mahowald, N. M.: Modeling mineral dust emissions from the Sahara desert using new surface properties and soil database, J. Geophys. Res., 113, D14218, doi:10.1029/2007JD009484, 2008. 27435

Largeron, Y., Guichard, F., Bouniol, D., Couvreux, F., Kergoat, L., and Marticorena, B.: On the importance of wind fields for dust emission over the Sahel, Geophys. Res. Lett., submitted, 2014.

Lothon, M., Saïd, F., Lohou, F., and Campistron, B.: Observation of the diurnal cycle in the low troposphere of West Africa, Mon. Weather Rev., 136, 3477, doi:10.1175/2008MWR2427.1, 2008. 27427

Marticorena, B. and Bergametti, G.: Modeling the atmospheric dust cycle: 1 Design of a soil derived dust production scheme, J. Geophys. Res., 100, 16415–16430, 1995a. 27432

Marticorena, B., Bergametti, G., Aumont, B., Callot, Y., N'doumé, C., and Legrand, M.: Modeling the atmospheric dust cycle: 2. Simulation of Saharan dust sources, J. Geophys. Res., 102, 4387–4404, doi:10.1029/96JD02964, 1997. 27432

Marticorena, B., Chatenet, B., Rajot, J. L., Traoré, S., Coulibaly, M., Diallo, A., Koné, I., Maman, A., NDiaye, T., and Zakou, A.: Temporal variability of mineral dust concentrations over West Africa: analyses of a pluriannual monitoring from the AMMA Sahelian Dust Transect, Atmos. Chem. Phys., 10, 8899–8915, doi:10.5194/acp-10-8899-2010, 2010. 27436

ACPD
14, 27425–27458, 2014

Marticorena, N. and Bergametti, G.: Modeling the atmospheric dust cycle: design of a soil-derived emission scheme, J. Geophys. Res., 102, 16415–16430, 1995b. 27427
Menut, L., Schmechtig, C., and Marticorena, B.: Sensitivity of the sandblasting fluxes calculations to the soil size distribution accuracy, J. Atmos. Ocean. Tech., 22, 1875–1884, 2005. 27432
Menut, L., Foret, G., and Bergametti, G.: Sensitivity of mineral dust concentrations to the model size distribution accuracy, J. Geophys. Res.-Atmos., 112, D10210, doi:10.1029/2006JD007766, 2007. 27433
Menut, L., Chiapello, I., and Moulin, C.: Previsibility of mineral dust concentrations: the CHIMERE-DUST forecast during the first AMMA experiment dry season, J. Geophys. Res., 114, D07202, doi:10.1029/2008JD010523, 2009. 27432
Menut, L., Bessagnet, B., Khvorostyanov, D., Beekmann, M., Blond, N., Colette, A., Coll, I., Curci, G., Foret, G., Hodzic, A., Mailler, S., Meleux, F., Monge, J.-L., Pison, I., Siour, G., Turquety, S., Valari, M., Vautard, R., and Vivanco, M. G.: CHIMERE 2013: a model for regional atmospheric composition modelling, Geosci. Model Dev., 6, 981–1028, doi:10.5194/gmd-6-981-2013, 2013. 27429, 27432
Moulin, C., Gordon, H. R., Banzon, V. F., and Evans, R. H.: Assessment of Saharan dust absorption in the visible from SeaWiFS imagery, J. Geophys. Res., 106, 18239, doi:10.1029/2000JD900812, 2001. 27437
Neggers, R. A. J.: A dual mass flux framework for boundary layer convection, Part II: Clouds, J. Atmos. Sci., 66, 1489–1506, 2009. 27429
Neggers, R. A. J., Köhler, M., and Beljaars, A. C. M.: A dual mass flux framework for boundary layer convection. Part I: Transport, J. Atmos. Sci., 66, 1465, doi:10.1175/2008JAS2635.1, 2009. 27429
Parker, D. J., Burton, R. R., Diongue-Niang, A., Ellis, R. J., Felton, M., Taylor, C. M., Thorncroft, C. D., Bessemoulin, P., and Tompkins, A. M.: The diurnal cycle of the West African monsoon circulation, Q. J. Roy. Meteor. Soc., 131, 2839–2860, doi:10.1256/qj.04.52, 2005. 27427, 27440
Pergaud, J., Masson, V., Malardel, S., and Couvreux, F.: A parameterization of dry thermals and shallow cumuli for mesoscale numerical weather prediction, Bound.-Lay. Meteorol., 132, 83–106, doi:10.1007/s10546-009-9388-0, 2009. 27428

ACPD
14, 27425–27458, 2014

Redelsperger, J.-L., Thorncroft, C. D., Diedhiou, A., Lebel, T., Parker, D. J., and Polcher, J.: African monsoon multidisciplinary analysis: an international research project and field campaign, B. Am. Meteorol. Soc., 87, 1739, doi:10.1175/BAMS-87-12-1739, 2006. 27436

Rio, C. and Hourdin, F.: A thermal plume model for the convective boundary layer: representation of cumulus clouds, J. Atmos. Sci., 65, 407–425, 2008. 27429, 27430

Rio, C., Hourdin, F., Grandpeix, J., and Lafore, J.: Shifting the diurnal cycle of parameterized deep convection over land, Geophys. Res. Lett., 36, 7809, doi:10.1029/2008GL036779, 2009. 27429

Rio, C., Hourdin, F., Couvreux, F., and Jam, A.: Resolved versus parametrized boundary-layer plumes, Part II: Continuous formulations of mixing rates for mass-flux schemes, Bound.-Lay. Meteorol., 135, 469–483, doi:10.1007/s10546-010-9478-z, 2010. 27431

Schepanski, K., Tegen, I., Todd, M. C., Heinold, B., BöNisch, G., Laurent, B., and Macke, A.: Meteorological processes forcing Saharan dust emission inferred from MSG-SEVIRI observations of subdaily dust source activation and numerical models, J. Geophys. Res.-Atmos., 114, D10201, doi:10.1029/2008JD010325, 2009. 27427

Seinfeld, J. H. and Pandis, S. N., eds.: Atmospheric Chemistry and Physics: From Air Pollution to Climate Change, in: Atmospheric chemistry and physics: from air pollution to climate change, New York, NY: Wiley, 1998 Physical description: xxvii, 1326 pp. A Wiley-Interscience Publication, ISBN: 0471178152, 1998. 27433

Shao, Y. and Lu, I.: A simple expression for wind erosion threshold friction velocity, J. Geophys. Res., 105, 22437–22443, 2000. 27432

Siebesma, A. P., Soares, P. M. M., and Teixeira, J.: A combined eddy-diffusivity mass-flux approach for the convective boundary layer, J. Atmos. Sci., 64, 1230, doi:10.1175/JAS3888.1, 2007. 27428

Slingo, A., Ackerman, T. P., Allan, R. P., Kassianov, E. I., McFarlane, S. A., Robinson, G. J., Barnard, J. C., Miller, M. A., Harries, J. E., Russell, J. E., and Dewitte, S.: Observations of the impact of a major Saharan dust storm on the atmospheric radiation balance, Geophys. Res. Lett., 33, L24817, doi:10.1029/2006GL027869, 2006. 27436

Soares, P. M. M., Miranda, P. M. A., Siebesma, A. P., and Teixeira, J.: An eddy-diffusivity/mass-flux parametrization for dry and shallow cumulus convection, Q. J. Roy. Meteor. Soc., 130, 3365–3383, 2004. 27428

ACPD
14, 27425–27458, 2014

Solmon, F., Mallet, M., Elguindi, N., Giorgi, F., Zakey, A., and Konaré, A.: Dust aerosol impact on regional precipitation over western Africa, mechanisms and sensitivity to absorption properties, Geophys. Res. Lett., 35, L24705, doi:10.1029/2008GL035900, 2008. 27426

Spyrou, C., Kallos, G., Mitsakou, C., Athanasiadis, P., Kalogeri, C., and Iacono, M. J.: Modeling the radiative effects of desert dust on weather and regional climate, Atmos. Chem. Phys., 13, 5489–5504, doi:10.5194/acp-13-5489-2013, 2013. 27427

Stull, R. B.: Transilient turbulence theory, Part I: The concept of eddy-mixing across finite distances, J. Atmos. Sci., 41, 3351–3367, 1984. 27428

Taylor, K. E., Stouffer, R. J., and Meehl, G. A.: An overview of CMIP5 and the experiment design, B. Am. Meteorol. Soc., 93, 485–498, doi:10.1175/BAMS-D-11-00094.1, 2012. 27427

Todd, M. C., Bou Karam, D., Cavazos, C., Bouet, C., Heinold, B., Baldasano, J. M., Cautenet, G., Koren, I., Perez, C., Solmon, F., Tegen, I., Tulet, P., Washington, R., and Zakey, A.: Quantifying uncertainty in estimates of mineral dust flux: an intercomparison of model performance over the Bodélé Depression, northern Chad, J. Geophys. Res.-Atmos., 113, D24107, doi:10.1029/2008JD010476, 2008. 27427, 27428, 27443

Troen, I. and Mahrt, L.: A simple model of the atmospheric boundary layer: sensitivity to surface evaporation, Bound.-Lay. Meteorol., 37, 129–148, 1986. 27428

Yamada, T.: Simulations of nocturnal drainage flows by a q^2/ turbulence closure model, J. Atmos. Sci., 40, 91–106, 1983. 27430

Yoshioka, M., Mahowald, N. M., Conley, A. J., Collins, W. D., Fillmore, D. W., Zender, C. S., and Coleman, D. B.: Impact of desert dust radiative forcing on sahel precipitation: relative importance of dust compared to sea surface temperature variations, vegetation changes, and greenhouse gas warming, J. Climate, 20, 1445, doi:10.1175/JCLI4056.1, 2007. 27426

ACPD
14, 27425–27458, 2014

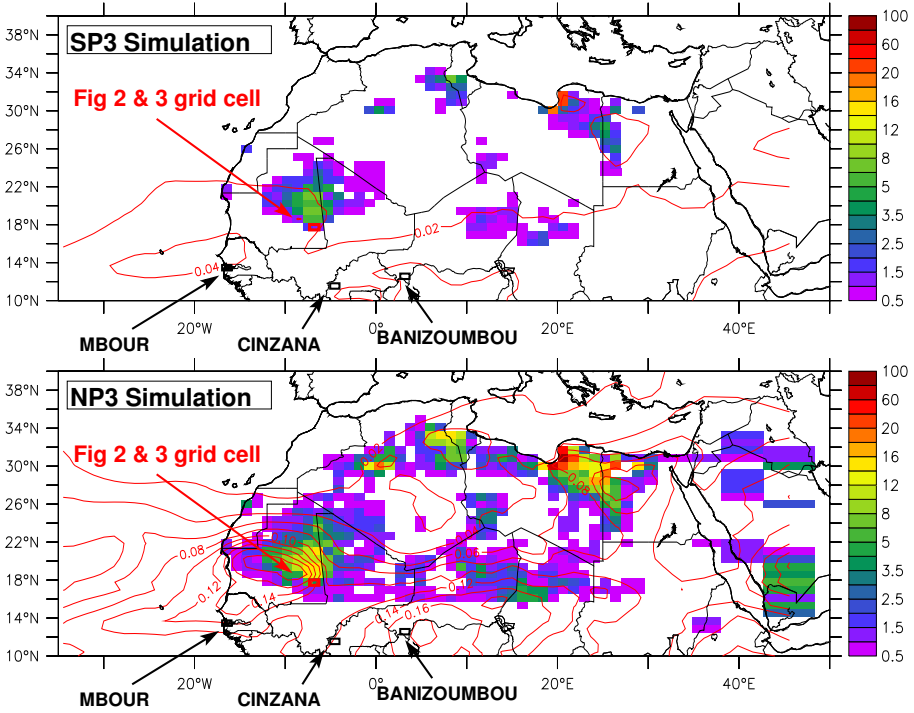

Figure 1. Comparison of the total emission ($\mu g\,m^{-2}\,s^{-1}$) for the SP3 (top) and NP3 (bottom) simulations (NP and SP versions of the physical package with τ = 3 h for nudging) for March 2006. Contours correspond to the mean AOT at 550 nm, with a 0.02 interval between contours.

ACPD
14, 27425–27458, 2014

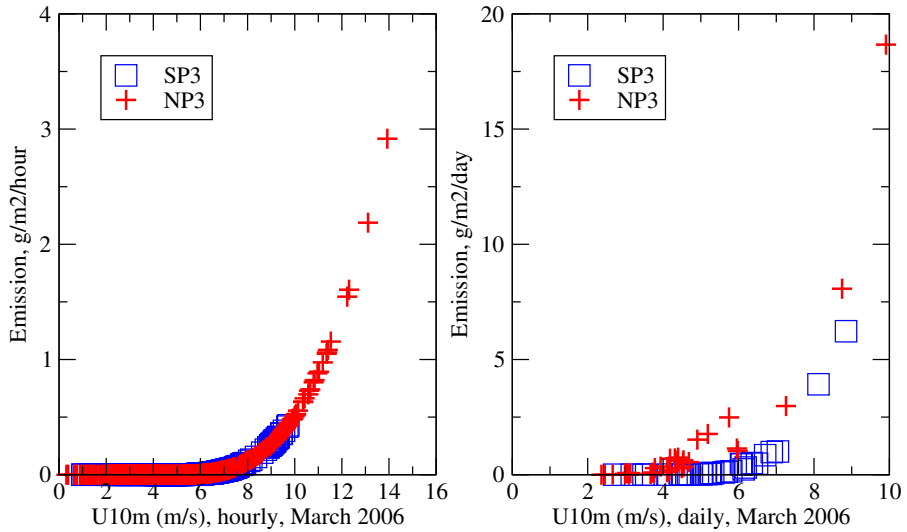

Figure 2. Scatter plot of the emission vs. 10 m wind speed ($m\,s^{-1}$) for simulations SP3 (blue) and NP3 (red) for March 2006, at (7.5° W, 18.5° N) (location shown in red in Fig. 1). The left panel corresponds to an hourly sampling of instantaneous values (with emission given in $g\,m^{-2}\,h^{-1}$) while the right panel is made from daily averages (with emissions given in $g\,m^{-2}\,day^{-1}$).

ACPD
14, 27425–27458, 2014

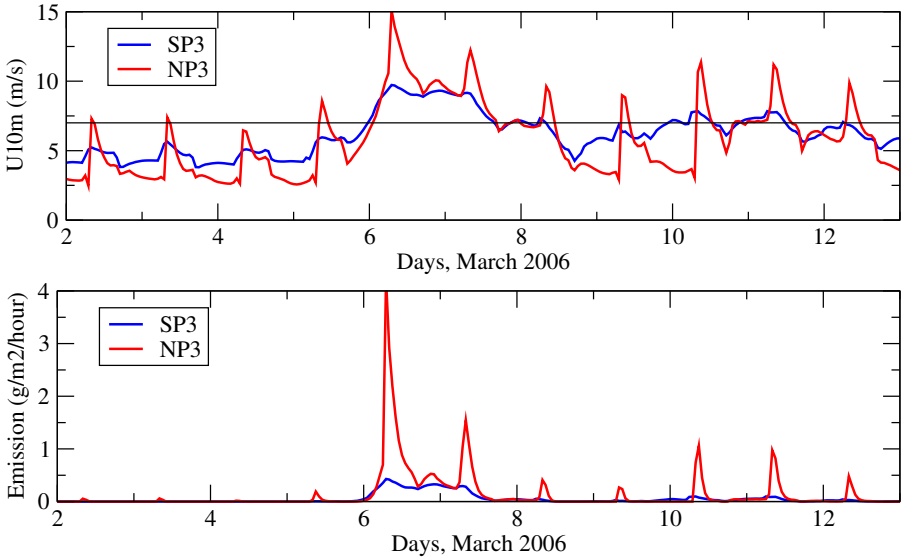

Figure 3. Comparison from 2 to 13 March 2006 of the 10 m wind (upper panel, $m\,s^{-1}$) and emission (lower panel, $g\,m^{-2}\,h^{-1}$) for simulations SP3 (blue) and NP3 (red) in the grid cell selected for emission analysis at (7.5° W, 18.5° N) (shown in red in Fig. 1).

ACPD
14, 27425–27458, 2014

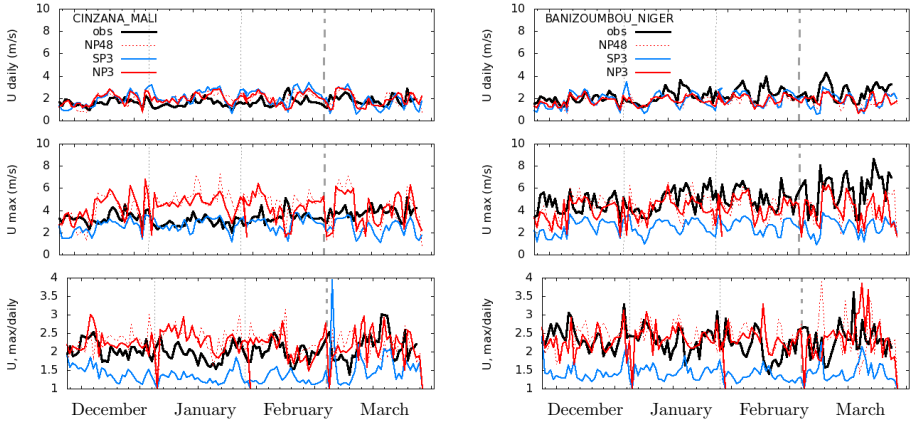

Figure 4. Time evolution over winter 2006 of the daily mean (upper panels) and maximum (mid panels) 10 m wind speed ($m\,s^{-1}$) as well as the ratio (lower panels) of the maximum value to the daily mean for Cinzana (left) and Banizoumbou (right). Results of the SP3 (blue), NP3 (red) and NP48 (red dashed) simulations are compared to site observations (black).

ACPD
14, 27425–27458, 2014

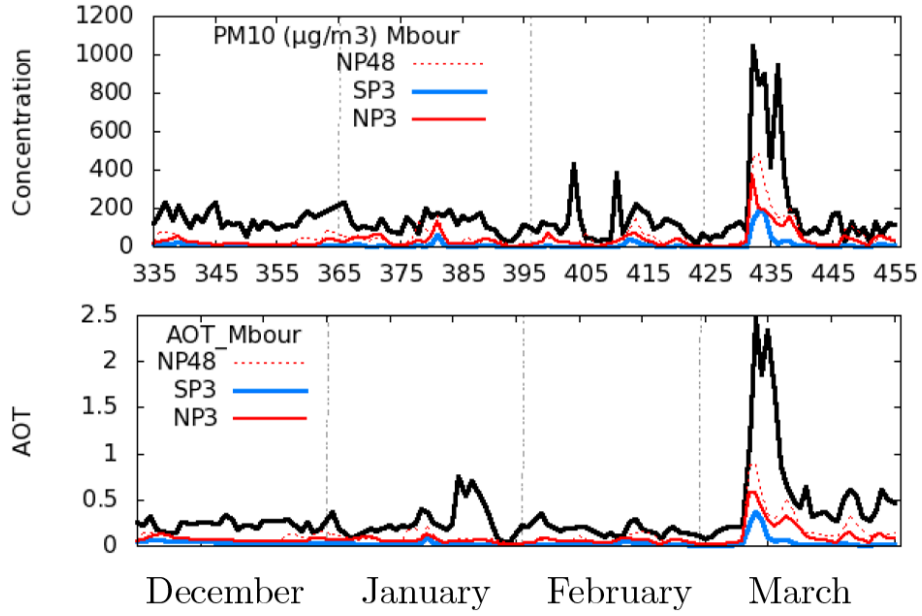

Figure 5. Time evolution over winter 2006, of the daily mean PM_{10} concentration (top, in $\mu g\,kg^{-1}$) and AOT for the M'bour station for simulations SP3 (blue), NP3 (red) and NP48 (red dashed) and for observations (black).

ACPD
14, 27425–27458, 2014

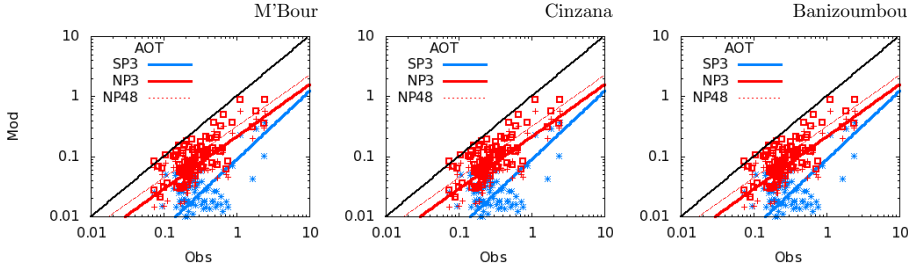

Figure 6. Scatter plots of the model vs. observed AOT at M'bour, Cinzana and Banizoubmou for simulations SP3 (blue), NP3 (red line and crosses) and NP48 (red dashed line and squares) computed at daily frequency.

ACPD
14, 27425–27458, 2014

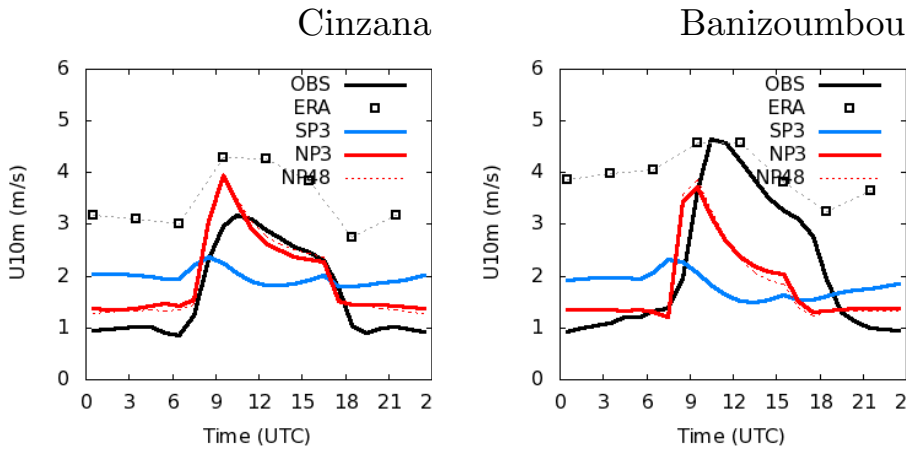

Figure 7. Wind mean diurnal cycle for DJFM of winter 2005–2006 ($m\,s^{-1}$) for the Cinzana (left) and Banizoumbou (right) stations. Model results (colored curves) are compared to observations (black curve) and ERAI reanalyzes (squares) for the same time period. Note that the universal and local times do not depart by more than one hour for the region considered here.

ACPD
14, 27425–27458, 2014

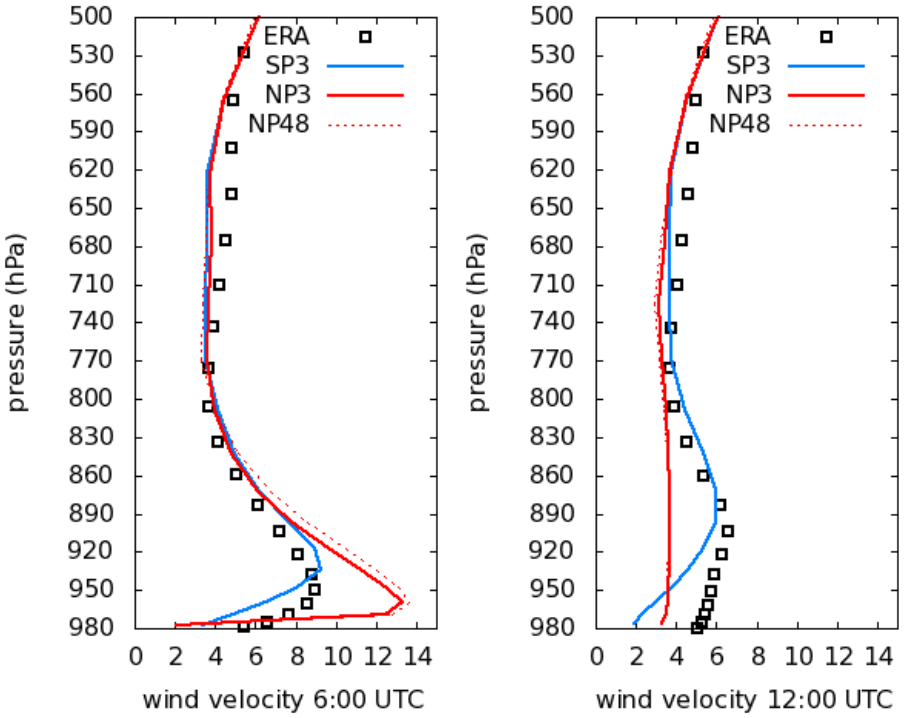

Figure 8. Wind mean vertical profiles ($m\,s^{-1}$) for DJFM of winter 2005–2006 at 06:00 and 12:00 UTC at Banizoumbou. Model results (colored curves) are compared to ERAI (black squares) for the same time period.

ACPD
14, 27425–27458, 2014

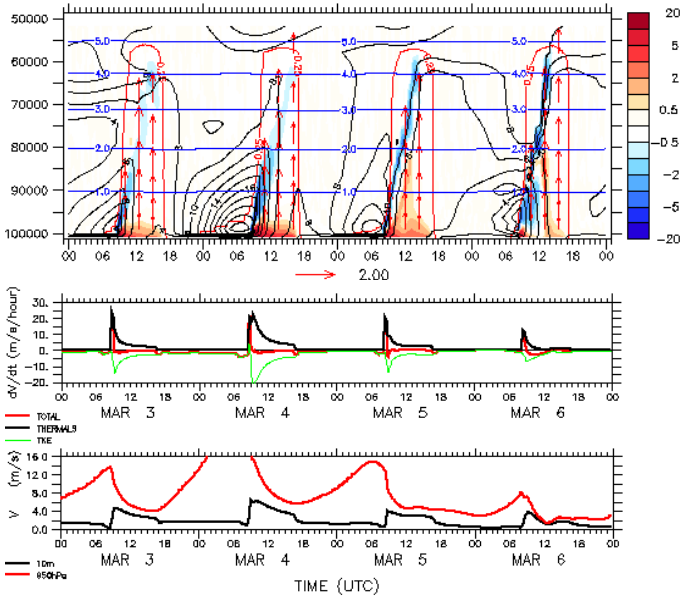

Figure 9. Four consecutive days showing the diurnal cycle of the boundary layer at Banizoumbou, in early March 2006. Are shown in the upper panel: the vertical distribution of the module of the horizontal wind (black contours, $m\,s^{-1}$), the wind module tendency due to vertical transport by the thermal plume model, according to Eq. (6) (colored shades with absolute iso-values 0.5, 1, 2, 3, 5, 10 and 20 $m\,s^{-1}\,h^{-1}$). The red contour delimits the depth of the boundary layer and corresponds to the 0.25 value of the bulk Richardson number (Eq. 7). The red arrows correspond to the thermal plume velocity in $m\,s^{-1}$ (under-sampled with respect to the space–time discretization of the simulation). The vertical axis, in pressure (Pa), and the altitude (in km, blue contours) are also shown. In the middle panel, we show for the first model layer (located at about 30 m above surface) the decomposition of the total wind module tendency (TOTAL, red, $m\,s^{-1}\,h^{-1}$) as the sum of the thermal plume contribution (THERMAS, black) and turbulent diffusion (TKE, green). The lower panel shows the wind speed at 10 m (black) and 950 hPa (red), close to the altitude where the nocturnal jet reaches its maximum.

ACPD
14, 27425–27458, 2014